

# Solid-state bonding of alloy-designed Cu–Zn brass and steel associated with phase transformation by spark plasma sintering

Naoya Masahashi · Satoshi Semboshi ·  
Kenichi Watanabe · Yuichi Higuchi ·  
Hideki Yamagata · Yoshitomo Ishizaki

Received: 10 February 2013 / Accepted: 9 April 2013 / Published online: 23 April 2013  
© The Author(s) 2013. This article is published with open access at Springerlink.com

**Abstract** Solid-state bonding between steel and a Cu alloy was studied to investigate fabrication of advanced bimetallic composites by using spark plasma sintering (SPS). In order to obtain proper bonding strength between the mating materials, Si and Al were alloyed to Cu–Zn brass to enhance interdiffusion with steel. The alloying elements diffused from the Cu alloy to steel, which transformed from the gamma to alpha phase during bonding. Owing to the phase stability of steel, the new columnar microstructure that evolved during the transformation across the joint interface showed high bonding strength between the mating alloys. The samples bonded without fracture, defects, or inhomogeneous deformation. Microstructural observations, elementary mapping, and mechanical testing demonstrated that the SPS technique and specific bonding parameters enhanced the interdiffusion between the metals. This novel method would be well suited to strengthen bonding between two dissimilar metals with different diffusion coefficients.

## Introduction

Bimetallic composites of dissimilar metals have been increasingly studied to satisfy a growing need for materials with unique mechanical, physical, and chemical properties [1–4]. A bimetallic strip of different metals with different

thermal expansion coefficients is widely called a “bimetal” and it has been used in thermometers, thermostats, glow lamps, and electromagnetic switches. The composite is fabricated by various methods such as clad rolling [5–8], diffusion bonding [9, 10], extrusion [11, 12], and sintering [13, 14], and the main issue for its fabrication is achieving high bonding strength between the mating metals. Mechanical bonding accompanied by plastic deformation is the most convenient method, while its drawback is low resistance to heavy loading, inhomogeneous deformation, and extreme atmospheres such as high temperatures and corrosive environments. Acceleration of interdiffusion between metals could overcome the weaknesses owing to strengthening of bonding across the joint interface. However, the high process temperatures and long-annealing times required to promote interdiffusion burden the fabrication process, and strong bonding is not expected intrinsically for combination of materials with low interdiffusion between them.

The spark plasma sintering (SPS) method is a well-known technique for powder sintering. It reduces sintering time and temperature and provides high densification when compared to conventional sintering [15]. The shortening of the sintering duration and lowering of the sintering temperature can be attributed to a microscopic electric discharge between the particles under pressure [16, 17]. In this study, SPS was applied to solid-state bonding between a Cu alloy and steel to obtain high bonding strength. Bimetallic composites of Cu and Fe have been used in the mechanical parts of axial piston pumps, which are utilized in applications for converting mechanical power into hydraulic power. An axial piston pump consists of multiple pistons in a circular array within a cylinder block born against the swash plate by means of slippers, and the surface of the slippers needs resistance against abrasive wear. The pistons themselves have to simultaneously endure high torque

N. Masahashi (✉) · S. Semboshi  
Institute of for Materials Research, Tohoku University,  
2-1-1 Katahira, Aoba, Sendai, Miyagi 980-8577, Japan  
e-mail: masahasi@imr.tohoku.ac.jp

K. Watanabe · Y. Higuchi · H. Yamagata · Y. Ishizaki  
Takako Industries Inc., 1-32-1 Housono-Nishi, Seika-Cho,  
Soraku-Gun, Kyoto 619-0240, Japan

strength to respond to high-load operations. The practical bimetallic composite of the slipper (Cu alloy) and the piston (steel) is fabricated by mechanical bonding, although it exhibits poor resistance to high-stress loading owing to low bonding strength. Several literatures concerning solid-state bonding of dissimilar metals by SPS have been reported [18–20], while the incorporation of Cu alloy with steel has not been reported thus far.

Extensive experimental studies on the impurity diffusion coefficient of Cu in Fe [21–24] and Fe in Cu [25–29] are summarized that the diffusion coefficient of Cu in Fe is several orders of magnitude lower than that of Fe in Cu. These experimental results are in agreement with simulations by the Diffusion-Controlled Transformation (DICTRA) software [30, 31]. On the other hand, Fe and Cu mutually dissolve in each other to a certain degree at high temperature; the solubility limit of Cu in Fe is 1.9 at.% at 1123 K and that of Fe in Cu is 4.6 at.% at 1369 K. This data suggest that it is difficult to achieve durable bonding between Cu and Fe via conventional diffusion.

In this study, the Cu alloy was designed to enhance interdiffusion with steel. We have previously studied the diffusion bonding between an Fe–Al alloy and pure Fe, and have reported successful bonding and subsequent rolling without fracture and warp. When the Al concentration in Fe exceeded the solubility limit in the gamma phase at the bonding temperature, a columnar microstructure developed on the steel side and provided high bonding strength [32, 33]. The mechanism of the columnar microstructure's evolution was understood in terms of the transformation from the gamma to alpha phase in steel during bonding, which was caused by Al diffusion from the Fe–Al alloy to steel [33]. Aluminum alloying restricts the formation of FCC structure iron (gamma), causing the gamma area of the phase diagram to contract to a small area referred as the gamma loop. This means that Al is encouraging the formation of BCC structure iron (alpha), and one result is that the delta- and alpha-phase fields become continuous. The gamma loop in the Fe–Al binary phase diagram (Fig. 1a) limits the Al solubility in the gamma phase and an Al concentration above the solubility limit causes transformation to the alpha phase [34]. In this study, this concept was applied to the coupling of steel with a Cu alloy, where Si and Al alloyed to Cu would diffuse to and then cause transformation in the steel. The Fe–Si binary phase diagram also has a gamma loop similar to the one in the Fe–Al binary phase diagram as shown in Fig. 1b [35]. The solubility of Si and Al in gamma Fe are 3.7 at.% at 1433 K and 2.4 at.% at 1411 K, respectively; their solubility in alpha Fe are 19.2 at.% at 1553 K and 55.0 at.% at 1338 K, respectively. When the concentrations of both elements diffusing from the Cu alloy to steel exceed the solubility limit in gamma Fe, transformation from the gamma to alpha phase should occur. Alpha nucleation followed by grain growth

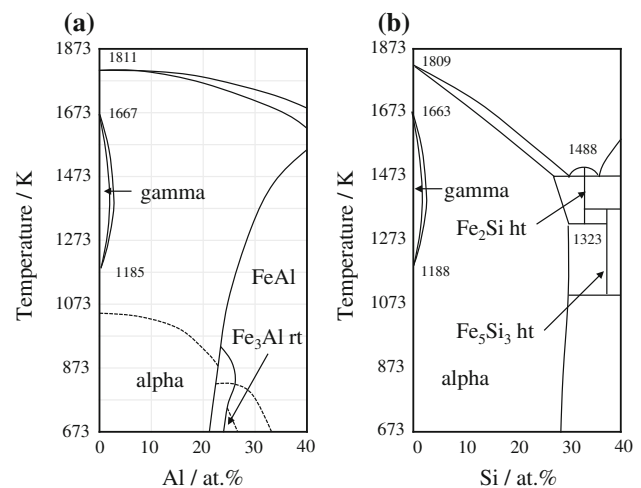


**Fig. 1** Portion of the Fe-rich (a) Fe–Al and (b) Fe–Si binary phase diagram

produces a new microstructure, which develops with a concentration gradient of Si and Al. Consequently, a columnar microstructural evolution across the joint interface is achieved and a high bonding strength is expected. The purpose of this study is to produce a bimetallic composite of the Cu alloy and steel with high bonding strength by SPS, with special focus on evolution of the new microstructure induced by the transformation.

## Experimental procedures

Cu–Zn brass alloyed with Al and Si (described as the Cu alloy hereafter) and heat-resistant steel (described as SCM435 hereafter) were used in this study. The Cu alloy ingot was prepared by high frequency induction furnace melting, and it was extruded to round bar at 873 K. The mechanical properties of the materials are as following; tensile strength, yield strength, tensile elongation, and Vickers hardness are 672, 315 MPa, 17 % and 180 Hv for Cu alloy, and 985 MPa, 817 MPa, 15 % and 318 Hv for SCM435. Figure 2 shows the microstructure (a) and energy-dispersive X-ray spectrometry (EDS) elementary mapping of Al (b), Cu (c), Fe (d), Si (e), and Zn (f) in the Cu alloy, revealing a dual phase of Cu solid solution and precipitation with high Fe, Al, and Si concentrations; the compositions of the precipitate and the matrix marked by +A and +B in Fig. 2 were 33.6Al–27.4Si–11.4Fe–20.5Ni–4.4Cu–2.7Zn and 8.4Al–1.4Si–0.4Fe–1.8Ni–60.9Cu–27.1Zn in at.%, respectively. On the other hand, SCM435 exhibited a deformed microstructure of bcc ferrite. The chemical compositions are tabulated in Table 1, where Si, C, and other components were analyzed by absorption spectroscopy, infrared spectroscopy, and inductively coupled plasma mass spectroscopy (ICP–MS), respectively. The Cu alloy

(20 mm  $\phi$ , 2 mm thickness) was placed on SCM435 (20 mm  $\phi$ , 20 mm thickness) for SPS bonding. The contact surface was ground with 1500-grade SiC paper, followed by ultrasonic cleaning in ethanol. The specimen was set into a graphite die with an internal  $\phi$  of 20.1 mm and bonded using a spark plasma sintering system (Dr. Sinter SPS-1050T, Sumitomo Coal Mining Co. Ltd., Japan). The specimen was heated to 873 K at a heating rate of about 100 K/min with a holding time of 3 min, followed by 50 K/min to 973 K, 20 K/min to 1023 K, 10 K/min to 1073 or 1103 K. The bonding was conducted at 1023, 1073, and 1103 K for 10 or 30 min in vacuum of  $\sim 6$  Pa, followed by nitrogen gas cooling. The temperature was controlled by a thermocouple inserted in the graphite die (positioned near the bonding interface). A uniaxial pressure of 20 MPa was applied on the sample through a graphite punch with 20 mm  $\phi$ ; the pressure was maintained at 20 MPa during bonding.

When the mating materials were bonded, the composite was cut into two pieces perpendicular to the joint interface. The cut surface was polished mechanically, followed by chemical polishing using a colloidal silica suspension with a particle size of approximately 0.04  $\mu\text{m}$ . The specimen was submitted for scanning electron microscopy (SEM) observation and

SEM–EDS analysis (XL 30 FEG, Phillips, The Netherlands). An exfoliation test specimen measuring 8 mm  $\phi$  in the loading part and 1.7 mm  $\phi$  in the axial shaft was prepared by wire-cut electrical discharge machining, where the joint interface was positioned in the axial shaft, as shown in Fig. 3. The bonding strength was determined by an exfoliation test using a universal mechanical strength tester (Romulus, Quad Group, USA), and the fractured surface was observed by SEM.

## Results

### Microstructure observation

All spark-plasma-sintered samples were bonded properly without fracture or inhomogeneous deformation. SEM micrographs in the interface vicinity of the samples are shown in Fig. 4. The samples shown were bonded at 1023 K for 10 min (Fig. 4a) and 30 min (Fig. 4b), at 1073 K for 30 min (Fig. 4c), and at 1103 K for 30 min (Fig. 4d). The original joint interface is not observed clearly, and the position of the interface marked by arrows is determined by measuring the distance from the opposite

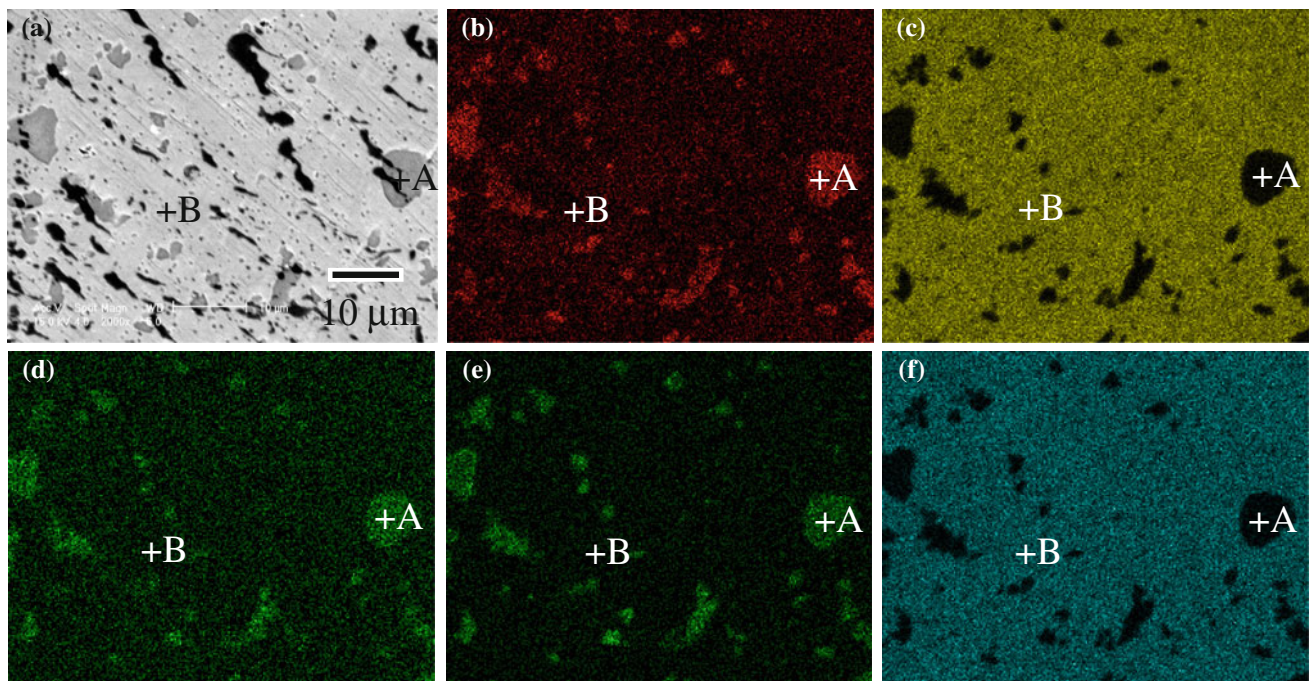


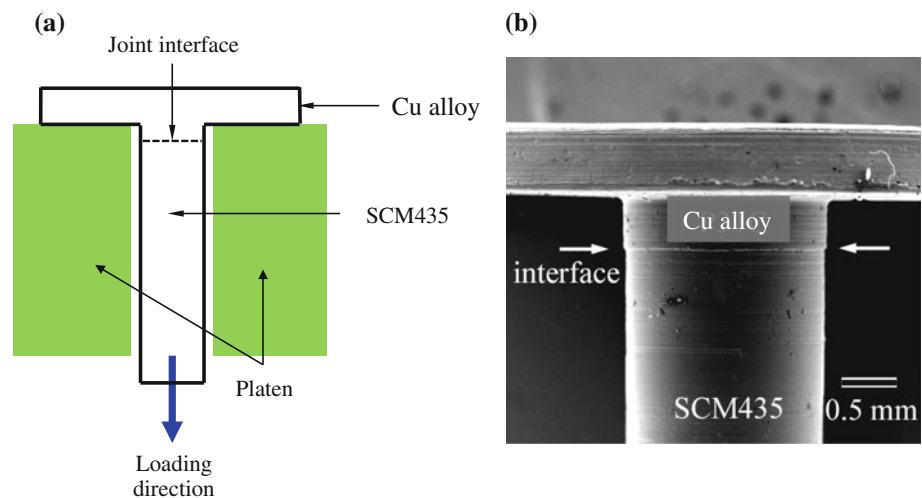
**Fig. 2** SEM micrograph (a) and EDS elementary mapping of Al (b), Cu (c), Fe (d), Si (e), and Zn (f) in the Cu alloy

**Table 1** Summary of chemically analyzed compositions in wt.% (at.% in parentheses)

Material	Fe	Al	Si	Cr	Zn	Cu	C	Mo	Ni
SCM435	97.3 (96.3)	0.1 (0.2)	0.2 (0.4)	1.2 (1.2)	–	–	0.4 (1.7)	0.2 (0.1)	0.1 (0.1)
Cu alloy	0.7 (0.8)	3.7 (8.2)	0.8 (1.7)	–	28.5 (25.0)	66.2 (61.4)	–	–	2.8 (2.9)



**Fig. 3** Schematic illustration of (a) the exfoliation test and (b) photo of its specimen



side of the joint face and marking the facing corner of each mating material by sharpening. A columnar microstructure evolved from the interface to the Cu alloy side, and a few micrometers of the second phase, as shown in the raw Cu alloy (Fig. 2), was observed on the Cu alloy side of the composite. The width of the columnar grain in Fig. 4b was wider than that in Fig. 4a, while it decreased with bonding

temperature. Kirkendall voids were observed near the front of the columnar grains on the Cu alloy side, suggesting that diffused flux of the Cu alloy is larger than that of SCM435. This is explained by the solid affinity between both alloying elements (Al and Si) and Fe due to the phase stability, which enhances their diffusion from the Cu alloy to SCM435.

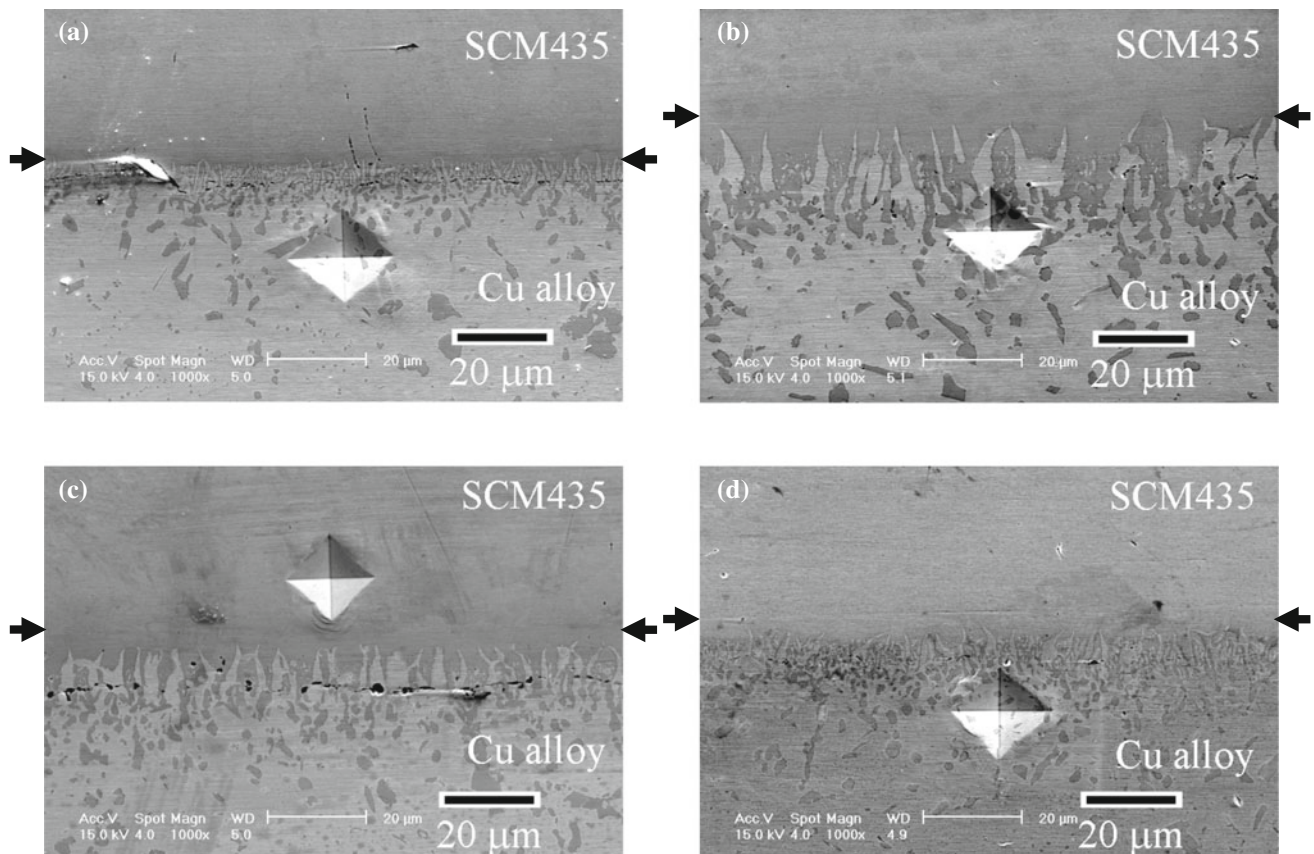


**Fig. 4** SEM micrographs in the interface vicinity of the sample that bonded at (a) 1023 K for 10 min, (b) 1023 K for 30 min, (c) 1073 K for 30 min, and (d) 1103 K for 30 min

## EDS analysis

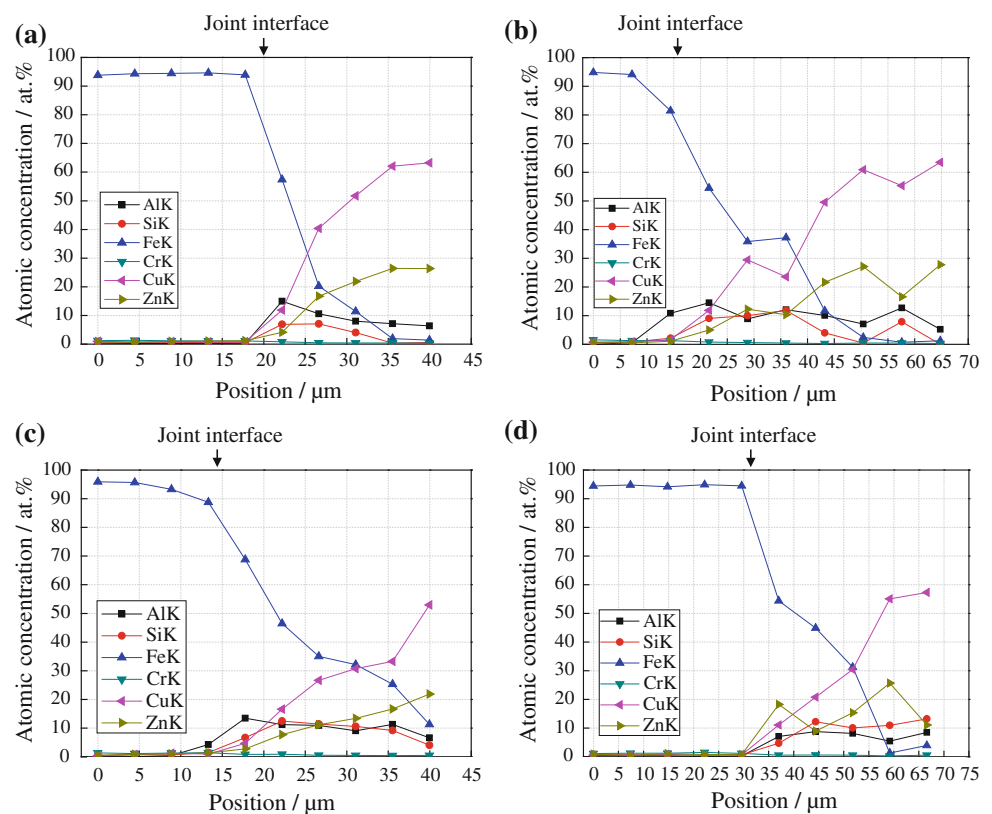
Figure 5 displays the EDS line profiles of the samples bonded at 1023 K for 10 and 30 min, at 1073 K for 30 min, and at 1103 K for 30 min. A continuous change in the concentration of the constituent elements, without any intermediate phases, was found across the interface. Fe diffused to the Cu alloy side, while Cu did not diffuse to SCM435. Si and Al diffused from the Cu alloy to SCM435, and concentrated on the Cu alloy side near the joint interface. The concentrations were lower than the nominal Si (1.7 at.%) and Al (8.2 at.%) compositions of the Cu alloy. Figure 6 shows the EDS elementary mapping of the samples that bonded at 1023 K for 10 and 30 min, at 1073 K for 30 min and at 1103 K for 30 min, revealing high Fe, Si, and Al content with Cu descending in the columnar grains and precipitates. The results were supported by point analysis of the sample that bonded at 1023 K for 30 min and at 1103 K for 30 min, as shown in Fig. 7a, b, respectively, where the joint interface is shown by arrows. The dark contrast area of the columnar grains and precipitates corresponded to high concentrations of Fe, Al, and Si, while the bright area corresponded to high concentrations of Cu and Zn. At point 1 in Fig. 7a or point 2 in Fig. 7b located near the joint interface, the concentrations of Al and Si were high. Similarly, the concentrations of Al and Si were high at point 4 in Fig. 7a and point

4 in Fig. 7b located far from the joint interface. Compared to the nominal concentrations (Table 1), Si was more enriched than Al in these regions. As a result, the alloying elements were distributed in correlation with the microstructure and the distributions are not related to their distance from the interface.

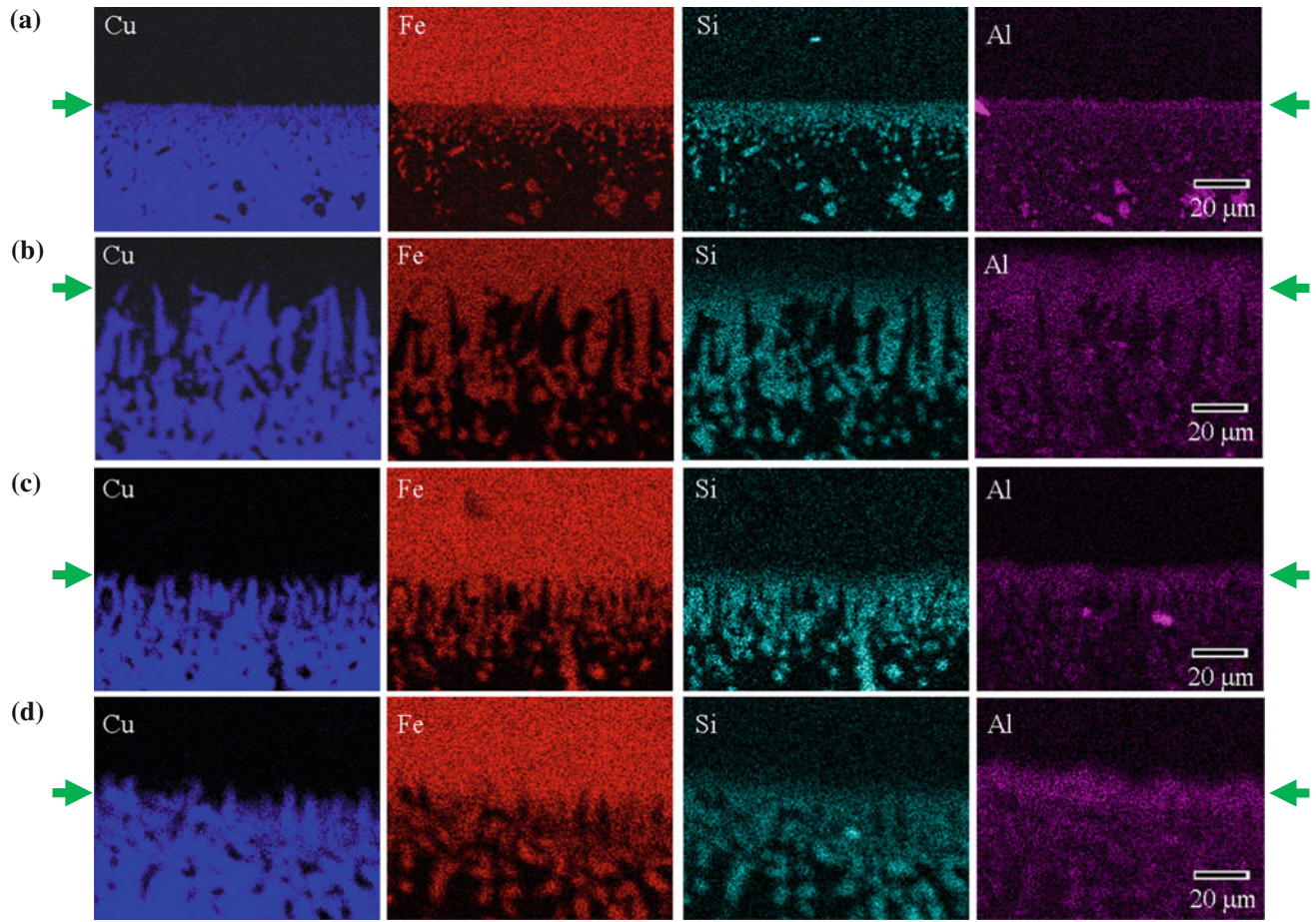
## Bonding strength

Table 2 summarizes the results of the exfoliation test, and plastic deformation was not observed in the stress–strain curves of all the samples. The samples that bonded at temperatures of 1023, 1073, and 1103 K for 30 min were not fractured up to the measurement limit of the equipment. On the other hand, the sample that bonded at 1023 K for 10 min fractured on the Cu alloy side. Figure 8 shows the side-view and fractured surface of the exfoliated sample that bonded at 1023 K for 10 min. The fractured position was located on the Cu alloy side near the joint interface, as shown in Fig. 8a; most of the fractured surface was occupied by the Cu alloy except for the rim of the sample, as shown in Fig. 8b. Figure 8c, d are magnifications of the center of the fractured surface and the circled area, respectively, in Fig. 8b. The Cu alloy fractured intergranularly, as shown in Fig. 8c, whereas the rim or near-edge area of the fractured surface corresponded to the joint interface shown in Fig. 8d.

**Fig. 5** EDS line profile for the samples that bonded at (a) 1023 K for 10 min, (b) 1023 K for 30 min, (c) 1073 K for 30 min, (d) 1103 K for 30 min

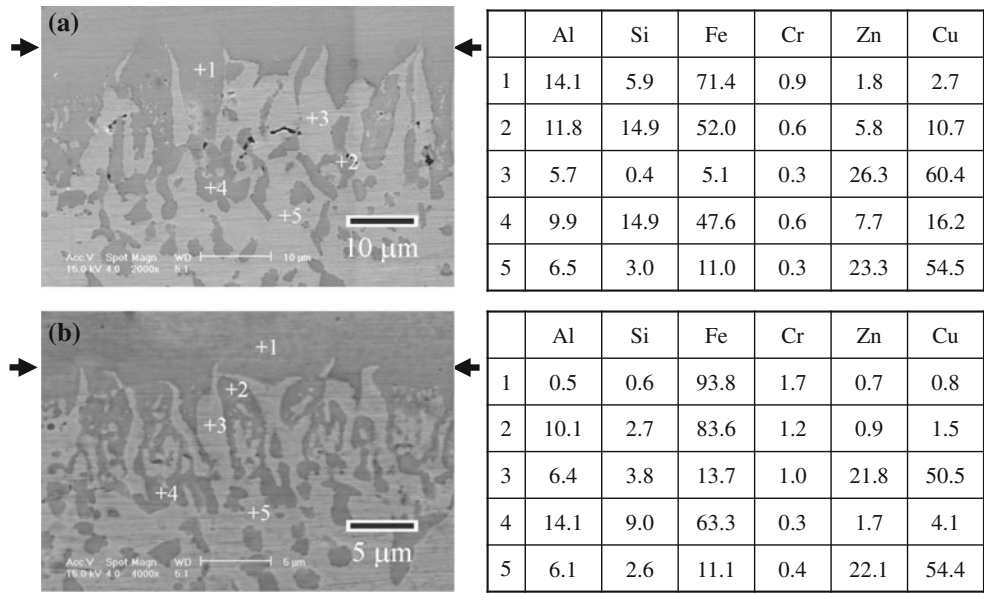






**Fig. 6** EDS elementary mapping of the samples that bonded at (a) 1023 K for 10 min, (b) 1023 K for 30 min, (c) 1073 K for 30 min, and (d) 1103 K for 30 min

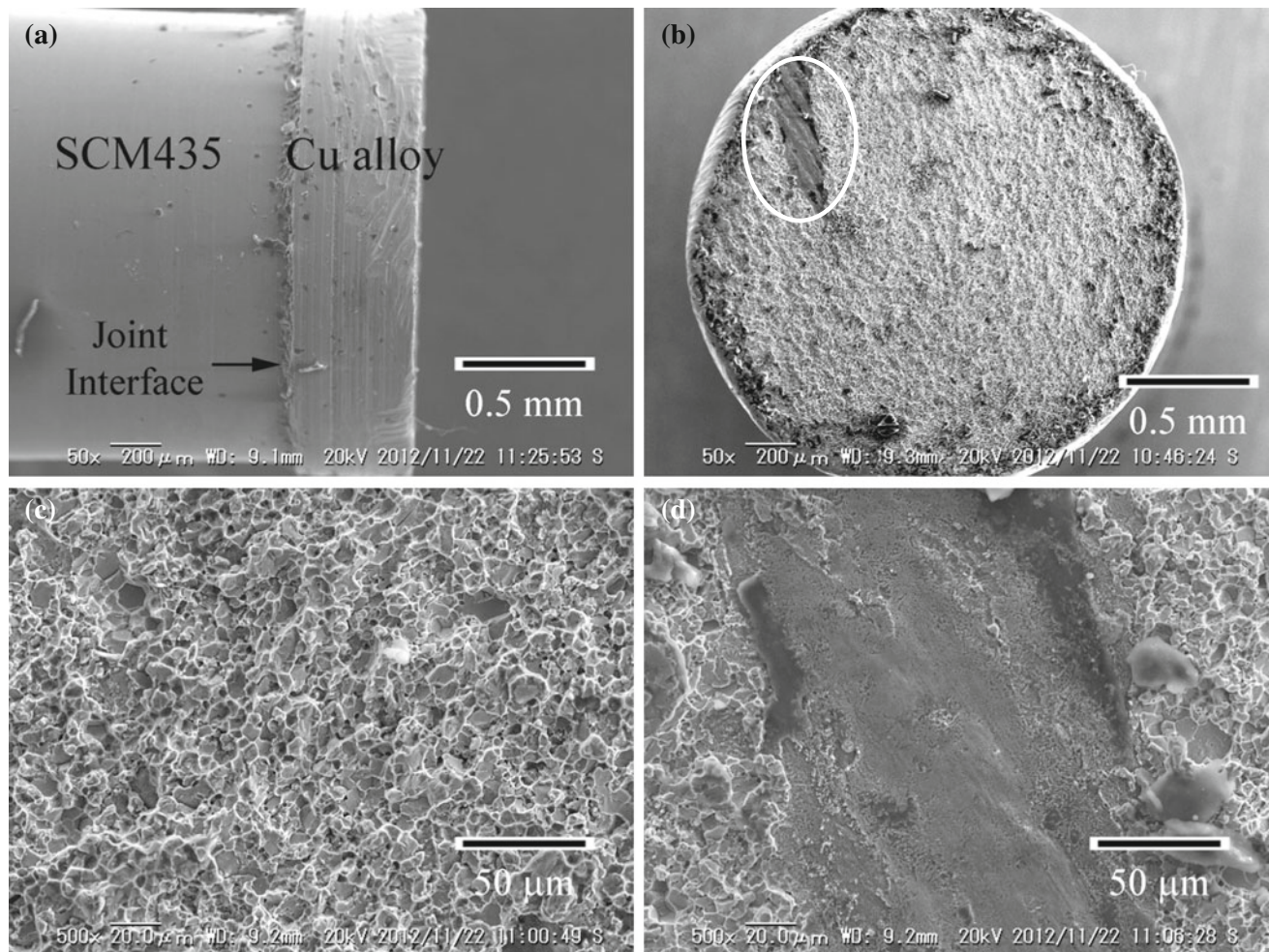
**Fig. 7** EDS point analysis of the sample that bonded at (a) 1023 K for 30 min and (b) 1103 K for 30 min





**Table 2** Summary of bonding strength determined by the exfoliation test

SPS conditions		Bonding strength/MPa	Fractured position
Temperature/K	Bonding time/min		
1023	10	215	Cu alloy
1023	30	>432	Not fractured
1073	30	>432	Not fractured
1103	30	>432	Not fractured

**Fig. 8** (a) Side-view and (b–d) fractured surface of the exfoliated sample that bonded at 1023 K for 10 min. Magnified view of the (c) center and (d) circled area in (b)

## Discussion

This study proved that the newly formed microstructure across the initial joint interface provided sound bonding between the mating materials. Si and Al were alloyed to Cu–Zn brass to initiate transformation from the gamma to alpha phase in steel, and the new microstructure evolved across the joint interface. EDS analysis revealed that both Si and Al were concentrated near the joint interface, and

both metals were alloyed with Fe that diffused from the SCM435 side. Consequently, different characteristic microstructures were formed in the Cu alloy near the joint interface; columnar grains originated from the transformed alpha nucleation and the second phase originated from the precipitates (Fig. 2). The interdiffusion coefficient of the alpha was several orders of magnitude higher than that of the gamma phase according to the interdiffusion coefficient in the Cu–Fe system [20, 36], which supported Fe diffusion

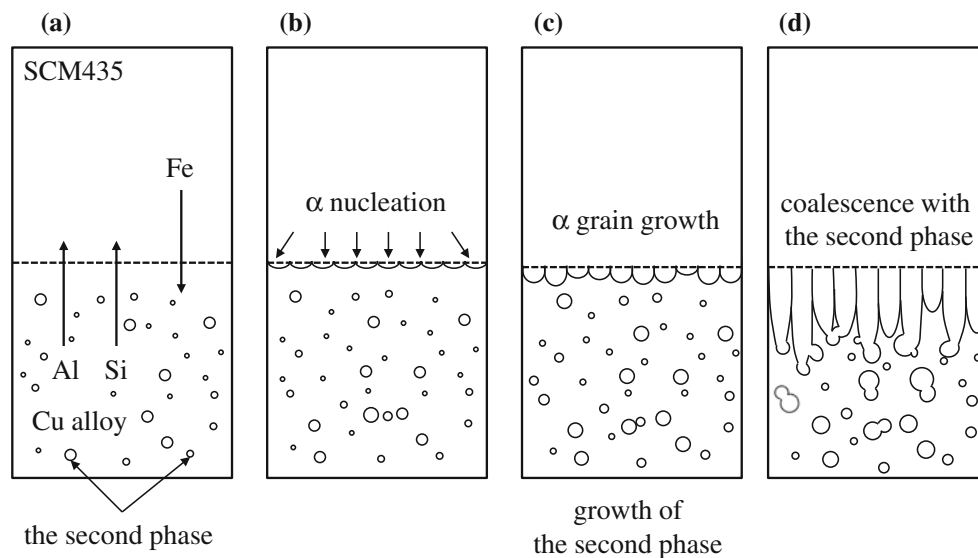


**Fig. 9** Illustration of the proposed model for microstructure evolution: (a) both Si and Al in the Cu alloy diffuse to the SCM435 side; (b) alpha nucleation near the joint interface; (c) grain growth to the

Cu alloy side; (d) grain growth accompanied by coalescence with precipitates in the Cu alloy

to the Cu alloy side. Figure 9 illustrates the proposed model for the present solid-state bonding. The current applied during SPS raised the sample temperature, and both Si and Al in the Cu alloy diffused near the joint interface toward the SCM435 side (Fig. 9a). When the concentrations of Si and Al exceeded the solubility limit of gamma steel in SCM435, transformation to alpha phase occurred (Fig. 9b), followed by alpha grain growth to the Cu alloy side (Fig. 9c). At the same time, the concentrated Si and Al near the joint interface alloyed with Fe that diffused from SCM435. With increasing bonding time, the columnar grains grew to the Cu alloy side, accompanied by coalescence with the second phase in the Cu alloy. The narrow width and short length of the columnar grains observed in the sample that bonded at 1103 K for 30 min (Fig. 4d) was attributed to the extended curve of the gamma loop in the Fe–Al or Fe–Si binary phase diagram (Fig. 1). In this case, the transformation was delayed due to the high concentrations of Al and Si required.

SPS enhances diffusion due to a microscopic electric discharge between the particles [16, 17], which enables powder sintering at low temperatures. It is noteworthy to mention that the controlled temperature monitored by a thermocouple installed in the graphite die is different from the actual temperature. The actual temperature of the sample should be higher than the controlled temperature, because the thermocouple cannot detect a local increase in temperature provided by a microscopic electric discharge between substances. A difference between the actual and controlled temperatures could be suppressed in metals but not in ceramics because of the metal's higher thermal conductivity. According to the temperature distribution calculation in the

powder compact and die, the higher the thermal conductivity of the sample, the lower the temperature difference [37, 38]. Thermal conduction analysis of powder sintering by SPS concluded that the local heat generation at the necked region was up to 200–300 K higher than the average temperature and it enhances the rapid densification and interparticle binding [39]. The present sample is not fabricated by powder sintering, but the local heating in the vicinity of joint interface is likely. The temperatures applied in this study 1023, 1073, and 1103 K were lower than the transformation temperature of Fe (1185 K). The actual temperature of the present sample should be higher than the controlled temperature, because the new microstructure proposed by the above-mentioned model should appear at a temperature above 1185 K. We estimate a difference of at least 160 K between the actual and the monitored temperatures.

We conclude that the evolved microstructure across the joint interface strengthened the bonding between the mating materials. The microstructure was formed by transformation in steel, which was initiated by alloy design to promote diffusion affecting steel's phase stability. The present study therefore provides a novel method to produce an advanced bimetallic composite.

## Conclusion

Solid-state bonding between steel and a Cu alloy with a composition designed to enhance diffusion based on phase stability of steel was conducted via SPS. The alloying elements Si and Al diffused from the Cu alloy to steel and caused transformation from the gamma to alpha phase. As



a result, a columnar microstructure evolved from steel to the Cu alloy across the joint interface, leading to high bonding strength between the mating alloys. The new microstructure evolution was explained by the proposed model based on transformation in conjunction with inter-diffusion of the constituents during bonding.

**Acknowledgements** The authors wish to acknowledge Mr. S. Sugiyama from IMR, Tohoku University for the sample preparations, Mr. A. Okubo from IMR, Tohoku University for the SPS experiments, and Mr. F. Sakamoto and Dr. T. Ashino from IMR, Tohoku University for the chemical analysis. We are grateful to Dr. Kim Nam Jae from PHOTOTECHNICA corporation for the exfoliation tests.

**Open Access** This article is distributed under the terms of the Creative Commons Attribution License which permits any use, distribution, and reproduction in any medium, provided the original author(s) and the source are credited.

## References

- Belyaev S, Rubanik V, Resnina N, Rubanik V, Rubanik O, Borisov V, Lomakin I (2010) *Phys Procedia* 10:52
- Peng J, Liu Z, Xia P, Lin M, Zeng S (2012) *Mater Lett* 74:89
- Tie LR, Xiang X, Sheng CF, Zhong LJ, Ling HL, Qing ZY (2011) *Tribol Inter* 44:101
- Abbasi M, Karimi Taheri A, Salehi MT (2011) *J Alloy Compd* 319:233
- Masahashi N, Komatsu K, Watanabe S, Hanada S (2004) *J. Alloy Compd* 379:272
- Berski S, Dyja H, Maranda A, Nowaczewski J, Banaszek G (2006) *J Mater Process Technol* 177:582
- Nezhad MS, Ardakani AH (2009) *Mater Des* 30:1103
- Chaudhari GP, Acoff V (2009) *Comp Sci Technol* 69:1667
- Yilmaz O, Çelik H (2003) *J Mater Process Technol* 141:67
- Ghosh M, Das S, Banarjee PS, Chatterjee S (2005) *Mater Sci Eng A* 390:217
- Mamalis AG, Szalay A, Vaxevanadis NM, Manolakos DE (1998) *J Mater Process Technol* 83:48
- Kazanowski P, Epler ME, Misiolek WZ (2004) *Mater Sci Eng A* 369:170
- Chang JH, Chou JM, Hsieh RI, Lee JL (2009) *Mater Chem Phys* 118:314
- Imgrund P, Rota A, Simchi A (2008) *J Mater Process Technol* 200:259
- Groza JR, Zavaliangos A (2000) *Mater Sci Eng A* 287:171
- Omori M (2000) *Mater Sci Eng A* 287:183
- Duan RG, Zhan GD, Kuntz JD, Kear BH, Mukherjee AK (2004) *Mater Sci Eng A* 373:180
- Nakamura T, Hayakawa K, Tanaka S, Imaizumi H, Nakagawa Y (2005) *Mater Trans* 46:292
- Hirose T, Shiba K, Ando M, Enoda M, Akiba M (2006) *Fusion Eng Des* 81:645
- Miriyev A, Stern A, Tuval E, Kalabukhov S, Hooper Z, Frage N (2013) *J Mater Process Technol* 213:161
- Lazarev VA, Golikov VM (1970) *Phys Met Metallorg* 29:154
- Salje G, Feller-Kniepmeier M (1977) *J Appl Phys* 48:1833
- Tsuji S, Yamanaka K (1974) *J Jpn Inst Met* 38:415
- Rothman SJ, Peterson NL, Walter CM, Nowicki LJ (1968) *J Appl Phys* 39:5041
- Mackliet CA (1958) *Phys Rev* 109:1964
- Mullen JG (1961) *Phys Rev* 121:1649
- Sen SK, Dutt MB, Barua AK (1978) *Phys Status Solidi A* 45:657
- Almazouzi A, Macht MP, Naundorf V, Neumann G (1996) *Phys Rev B* 54:857
- Tomono Y, Ikushima A (1958) *J Phys Soc Jpn* 13:762
- Wanga S, Zhoua P, Zhanga W, Cui S, Zhanga L, Yin M, Liu D, Xua H, Liu S, Dua Y (2012) *Calphad* 36:127
- Liu Y, Wang J, Duc Y, Zhang L, Liange D (2010) *Calphad* 34:253
- Masahashi N, Kondo N, Hanada S (2002) *Ann Chim Sci Mater* 27:S231
- Masahashi N, Watanabe S, Nomura N, Semboshi S, Hanada S (2005) *Intermetallics* 13:717
- Masahashi N, Hanada S (2004) *ISIJ Inter* 44:878
- ASM Alloy Phase Diagrams Center (2013). <http://www1.asminternational.org/asmenterprise/apd/>. Accessed 26 Jan 2013
- Speich GR, Gula JA, Fisher RM (1964) *J Electrochem Soc* 111:C203
- Yucheng W, Zhengyi F (2002) *Mater Sci Eng B* 90:34
- Tiwari D, Basu B, Biswas K (2009) *Ceram Inter* 35:699
- Saida K, Tsuduki R, Nishimoto K (2004) *J Jpn Inst Metal* 68:419